

Thermomigration of Au¹⁹⁵ and Sb¹²⁵ in Gold*†

WILLIS MOCK, JR.‡

Department of Physics and Materials Research Laboratory, University of Illinois, Urbana, Illinois 61801

(Received 16 September 1968)

The effect of large thermal gradients on the mass transport of Au¹⁹⁵ and Sb¹²⁵ in gold has been investigated. Specimens in the form of rods containing two welded interfaces separated by $\frac{1}{8}$ in. were fabricated. Each interface contained a layer of the appropriate tracer and an inert radioactive Hf¹⁸¹O₂ marker. The specimens were annealed in a vacuum furnace which provided a temperature gradient of approximately 300°C/cm. The radioactive penetration profiles at the hot and cold interfaces were determined experimentally by sectioning the specimen on a lathe and assaying the radioactivity in each section. The penetration profiles, which were skewed Gaussians, were curve-fitted by the method of least squares. The temperature at each interface and the temperature gradient were determined from the measured D values and the known tracer self-diffusion coefficients. During the temperature-gradient anneal, the maximum of the tracer profile at the hot interface shifted with respect to the Hf¹⁸¹O₂ marker. From the measured shift values, the heat of transport of Au¹⁹⁵ in gold was measured to be $Q^*_{Au} = 0.80 \pm 0.27$ eV, approximately equal to the vacancy migration energy. The heat of transport for Sb¹²⁵ in gold was found to be $Q^*_{Sb} = -2.02 \pm 0.23$ eV. These results indicate that the static temperature gradient dominates the thermomigration process of the solvent, while a charge-carrier-impurity interaction governs the process for the solute.

I. INTRODUCTION

IF a homogeneous binary alloy is placed in a temperature gradient a redistribution of the constituents can occur with one constituent migrating to the cold end of the specimen and the other to the hot end. This phenomenon, which is called thermomigration, was first investigated by Ludwig¹ and Soret² in gases and liquids. Only recently has the phenomenon been investigated in solids.

The basic macroscopic equations governing the phenomenon in solids are obtained from irreversible thermodynamics and have been discussed by several authors.^{3,4} For a pure solid containing vacancies the flux of vacancies with respect to the lattice in one dimension along the temperature gradient is given by

$$J_v = \frac{n_v D_v}{kT^2} (Q^* - \Delta H_F) \frac{dT}{dx}. \quad (1)$$

Here D_v is the vacancy diffusion coefficient, ΔH_F is the vacancy formation enthalpy, n_v is the local equilibrium vacancy concentration, T is the absolute temperature, dT/dx is the temperature gradient, k is Boltzmann's constant, and Q^* is the heat of transport of the solvent atoms. The heat of transport is defined as the flux of heat J_q transported by a unit mass

current J_m at constant temperature,

$$Q^* = (J_q/J_m)_{dT/dx=0}. \quad (2)$$

In a single-component system, to conserve lattice sites, $J_m = -J_v$. The net current of vacancies through the lattice will be toward higher temperatures if $Q^* - \Delta H_F$ is positive and toward lower temperatures if $Q^* - \Delta H_F$ is negative, whereas the net flow of atoms will be in the opposite direction. The net flux of atoms through the crystal gives rise to a motion of markers fixed to the crystal lattice with respect to the laboratory frame since lattice planes are created at one part of the crystal and destroyed at another. The markers will move in a direction opposite to that of the net current of atoms.

In the past, two methods for measuring the velocity of the crystal lattice have been used. One method⁵ consists of placing scratch marks on the specimen perpendicular to the temperature gradient and observing the relative motion of the marks with a microscope. The quantity $Q^* - \Delta H_F$ is determined from the relative distance change between the marks. This method suffers from at least two adverse effects. It is possible that the marks act as sources and sinks for vacancies in such a way that the observed net mass transport as measured by the marker movement is actually less than the actual mass transport which occurred. Another possible source of error is that surface diffusion effects taking place in the region of the scratch marks may govern their motion, rather than volume diffusion effects.

The second method⁶ for measuring the lattice movement is to sinter small inert wires into the volume of the crystal and observe the change in distance between the wires. The largest source of error in this method is improper bonding between the inclusion wires and the specimen, with the result that the wires do not move with the actual velocity of the lattice. In addition, void

* Supported in part by the U. S. Atomic Energy Commission under Contract AT(11-1)-1198.

† Based on a thesis submitted by Willis Mock, Jr., to the University of Illinois in partial fulfillment of the requirements for the degree of Doctor of Philosophy in Physics.

‡ Present address: U. S. Naval Weapons Laboratory, Dahlgren, Virginia 22448.

¹ C. Ludwig, Sitzber. Akad. Wiss. Wien, Math. Naturw. Kl. 20, 539 (1856).

² Ch. Soret, Arch. Genève 3, 48 (1879).

³ S. R. de Groot, *Thermodynamics of Irreversible Processes*, (Wiley-Interscience, Inc., New York, 1951).

⁴ Y. Adda and J. Philibert, *La Diffusion dans les Solides* (Institut National des Sciences et Techniques Nucleaires, Saclay, 1966).

⁵ D. Jaffe and P. G. Shewmon, Acta Met. 12, 515 (1964).

⁶ C. J. Meechan and G. W. Lehman, J. Appl. Phys. 33, 634 (1962).

growth and strain effects around the wire may influence the wire movement. These experimental errors are reflected in the results reported using these two methods. Positive, zero, and negative values for $Q^* - \Delta H_F$ have all been reported in the literature by different experimenters for both Cu⁵⁻⁷ and Zn.⁸⁻¹¹ In these and in other metals the errors reported could be as large as 100%.

The method of using internal radioactive markers and tracers, used previously for electromigration and Kirkendall effect experiments, obviates most of these difficulties. In this method, a thin layer of radioactive tracer is deposited on one surface of mating optical flats while the other surface is coated with an exceedingly small concentration of nondiffusing internal radioactive marker ($\frac{1}{10}$ atom layer). The flats are then welded together in a vacuum, and the specimen is placed in a temperature gradient for the diffusion anneal. After diffusion the specimen is sectioned on a precision lathe to determine directly the penetration profile of the tracer and the shift with respect to the internal marker.

This method has advantages over the previous two methods: First, the net flux of atoms through the bulk of the specimen is measured directly and is not affected by surface abnormalities; second, the internal marker which is used to mark the position of the lattice is a thin layer of radioactive isotope, and this would not introduce strain effects and vacancy precipitation as would an internal foreign body.

In the present experiment the thermomigration of Au¹⁹⁵ and Sb¹²⁵ in Au has been measured. The experiment was undertaken because no self-consistent data for self-thermomigration in Au exists. Another purpose for the experiment was to test the atomistic theory for thermomigration. Adda *et al.*⁷ using the method of marking the crystal lattice internally with a thin wire, observed no relative motion between the wire and a thin plate which marked the laboratory frame, indicating that, for Au, $Q^* - \Delta H_F = 0$. Meechan and Lehman⁶ obtained a value of -0.20 ± 0.15 eV using internal wires in one specimen, but in a second specimen a smaller marker movement was observed, while in a third, no marker movement was observed at all. Jaffe and Shewmon,⁵ using the scratch mark technique, obtained a value for $Q^* - \Delta H_F$ of -0.37 eV although it seems that this reported value should be decreased by about 20% because the diffusion correlation factor f was apparently neglected. Because of the inconsistency of these results, an accurate determination of self-thermo-

migration in Au is clearly desirable, since other defect properties of Au have received careful study.

No previous results for the thermomigration of Sb¹²⁵ in Au have been reported. These data, as well as the results for self-thermomigration in Au are essential to test atomistic theories for thermomigration which have been proposed by Huntington,¹² Gerl,¹³ and others.^{14,15}

In these models it is presumed that a solvent atom situated at the saddle-point position in a temperature gradient will experience three driving forces: A force due to the static temperature gradient, a force due to the thermoelectric field, and a force due to the heat carrier interaction. For single-band metals, the contribution due to the heat carrier interaction is presumed negligible, because, to maintain current neutrality, the flow of electrons or holes serving as heat carriers down the temperature gradient must be balanced by an equal flow of less energetic electrons or holes up the temperature gradient. The result is that the net interaction with moving charges should be small. Measurement of self-thermomigration in Au provides a test for this theory. On the other hand, the heat carrier interaction is predicted to be significant for substitutional impurities with a valence different from that of the solvent, as a result of the large scattering cross section of the impurity for charge carriers. Sb (valence 5) thermomigration in Au (valence 1) is therefore a good choice to test this part of the theory.

Following Huntington,¹² the heat of transport is written as the sum of three terms,

$$Q^* = Q_1^* + Q_2^* + Q_3^*, \quad (3)$$

where the three heats of transport on the right-hand side of the equation are due to the above-mentioned forces. The first term is the contribution due to the static temperature gradient. From the model of Wirtz¹⁶ and Brinkman,¹⁷

$$Q_1^* = \alpha\beta\Delta H_M; \quad (4)$$

ΔH_M is the vacancy migration energy, α is an enhancement factor because a phonon scattered by a vacancy will enhance the temperature gradient slightly, and β is a fraction which is predicted to about 0.8 or 0.9. A jumping atom is assumed to carry an energy $\beta\Delta H_M$ forward in the jump direction when it moves into a vacant site; the remainder of the migration energy, $(1-\beta)\Delta H_M$, is presumed localized in the motion of the saddle-point atoms. β is thus a measure of the distribution of the migration energy between normal modes when a jump occurs. Since α is approximately unity,

⁷ Y. Adda, G. Brebec, N. V. Doan, M. Gerl, and J. Philibert, International Atomic Energy Agency Report No. SM 66/52, 1966 (unpublished).

⁸ T. F. Archbold and P. G. McCormick, Trans. Met. Soc. AIME **236**, 713 (1966).

⁹ P. G. Shewmon, J. Chem. Phys. **29**, 1032 (1958).

¹⁰ H. G. Feller and H. Wever, J. Phys. Chem. Solids **24**, 969 (1963).

¹¹ R. A. Swalin, W. C. Olander, and P. Lin, Acta. Met. **13**, 1063 (1965).

¹² H. B. Huntington, Rensselaer Polytechnic Institute Report No. 1066-14, 1968 (unpublished).

¹³ M. Gerl, J. Phys. Chem. Solids **28**, 725 (1967).

¹⁴ R. A. Oriani, U. S. Steel Corp. Report No. 1406, 1968 (unpublished).

¹⁵ V. B. Fiks, Fiz. Tverd. Tela **5**, 3473 (1963) [English transl.: Soviet Phys.—Solid State **5**, 2549 (1964)].

¹⁶ K. Wirtz, Z. Physik **44**, 221 (1943).

¹⁷ J. A. Brinkman, Phys. Rev. **93**, 345 (1954).

Q_1^* is expected to be of the order of the migration energy.

The contribution due to the thermoelectric field¹⁵ is

$$Q_2^* = eZ\eta T, \quad (5)$$

where e is the magnitude of the electronic charge, Z is the charge number of the moving ion seen by the electrostatic field, and η is the Thompson coefficient. It has been difficult to predict a value for Z theoretically since it is a function of conduction electron screening. At ordinary diffusion temperatures Q_2^* is estimated to be smaller than 0.01 eV and thus is negligible compared to Q_1^* .

The contribution due to the charge carrier-ion interaction for a single-band metal is given by¹²

$$Q_3^* = [(\pi kT)^2 / 6E_F](n_e l \sigma_i). \quad (6)$$

E_F is the Fermi energy, n_e is the electron concentration, l is the mean free path for electrons, and σ_i is the scattering cross section for electrons by the activated complex. Huntington estimates this term to be less than 0.02 eV at diffusion temperatures for self-thermomigration of solvent atoms in single-band metals. This term is expected to be significant for solute motion in single-band metals (large σ_i) or for motion in multiband metals where a zero current condition can be maintained by flow of both electrons and holes in the same direction.

II. PHENOMENOLOGICAL EQUATIONS

A. Tracer Self-Thermomigration

Following the treatments by Adda⁴ and Lazarus,¹⁸ let A represent the solvent atoms and A^* represent the tracer atoms. Diffusion only along the x direction is considered. The general expressions for the flux of tracer atoms A^* and solvent atoms A in the lattice frame are given by⁴

$$J_{A^*} = -D_{A^*} \frac{\partial n_{A^*}}{\partial x} - [L_{A^*A^*}(Q_{A^*}^* - \Delta H_F) + L_{A^*A}(Q_A^* - \Delta H_F)] \frac{1}{T^2} \frac{dT}{dx}, \quad (7)$$

$$J_A = +D_A \frac{\partial n_A}{\partial x} - [L_{AA^*}(Q_{A^*}^* - \Delta H_F) + L_{AA}(Q_A^* - \Delta H_F)] \frac{1}{T^2} \frac{dT}{dx}. \quad (8)$$

Since the tracer and solvent atoms are chemically equivalent, $Q_{A^*}^* = Q_A^*$. The L 's are the phenomenological coefficients relating the fluxes to the driving forces of chemical potential gradient and temperature gradient.

Let n_{A^*} , n_A , n_v , and n represent the concentrations of tracer atoms, solvent atoms, vacancies and lattice

sites, respectively. These are related by the equation

$$n_A + n_{A^*} + n_v = n. \quad (9)$$

Since at constant temperature the total current $J_{A^*} + J_A = 0$, the coefficients D_{A^*} and D_A are equal. D_{A^*} is the tracer diffusion coefficient and is related to the self-diffusion coefficient by the correlation factor.

It is possible to obtain expressions for D_{A^*} and D_A in terms of the phenomenological coefficients

$$D_{A^*} = k[L_{A^*A^*}/n_{A^*} - L_{A^*A}/n_A], \quad (10)$$

$$D_A = k[L_{AA}/n_A - L_{AA^*}/n_{A^*}]. \quad (11)$$

The cross terms L_{AA^*} and L_{A^*A} are equal because of microscopic reversibility, but these terms cannot be neglected with respect to the diagonal terms $L_{A^*A^*}$ and L_{AA} because of correlation effects in the vacancy diffusion process.

Since $n_A \gg n_{A^*}$, $L_{A^*A^*}/n_{A^*} \gg L_{A^*A}/n_A$, thus Eqs. (10) and (11) reduce to

$$D_{A^*} = D_{A^*A^*}, \quad (12)$$

$$D_A = D_{AA} - D_{AA^*}. \quad (13)$$

But $D_{A^*} = D_A$, therefore

$$D_{A^*} = D_{AA} - D_{AA^*} = fD_{AA}. \quad (14)$$

D_{AA} is the self-diffusion coefficient and f is the correlation factor. Only the fcc lattice is involved in the present experiment and the correlation factor is 0.78 for this case.¹⁹

For the above relations, Eqs. (7) and (8) can be rewritten as

$$J_{A^*} = -D_{A^*} \frac{\partial n_{A^*}}{\partial x} - \frac{D_{AA} n_{A^*}}{kT^2} (Q_A^* - \Delta H_F) \frac{dT}{dx}, \quad (15)$$

$$J_A = +D_A \frac{\partial n_A}{\partial x} - \frac{D_{AA} n_A}{kT^2} (Q_A^* - \Delta H_F) \frac{dT}{dx}. \quad (16)$$

Equations (15) and (16) show that the tracer diffusion coefficient enters into the concentration gradient terms whereas the self-diffusion coefficient enters into the temperature gradient terms.

In order to determine the flux of tracer in the laboratory reference frame, the relative velocity of the two reference frames must be determined. This velocity, V , is given by

$$(n_A + n_{A^*})V = -(J_{A^*} + J_A). \quad (17)$$

Substituting the lattice flux Eqs. (15) and (16) gives

$$V = \frac{D_{A^*}}{fkT^2} (Q_A^* - \Delta H_F) \frac{dT}{dx}. \quad (18)$$

¹⁸ D. Lazarus, in *Energetics in Metallurgical Phenomena*, edited by W. M. Mueller and M. C. Shaw (Gordon and Breach Science Publishers, Inc., New York, 1965).

¹⁹ K. Compaan and Y. Haven, *Trans. Faraday Soc.* **54**, 1498 (1958).

The tracer diffusion coefficient and correlation factor have been substituted for the self-diffusion coefficient. This is the velocity expression that is usually used to measure the quantity $Q^* - \Delta H_F$ experimentally using the scratch mark and internal wire techniques.

The flux of tracer in the laboratory reference frame is given by

$$J_{A^*} = J_{A^*} + n_{A^*}V = -D_{A^*}(\partial n_{A^*}/\partial x). \quad (19)$$

This equation shows that there is actually no net flux of tracer atoms due to the temperature gradient in the laboratory frame, as required by consideration of momentum conservation.

To obtain the differential equation for the concentration of tracer atoms the continuity equation is used;

$$\frac{\partial n_{A^*}}{\partial t} = -\frac{\partial J_{A^*}}{\partial x} = D_{A^*} \frac{\partial^2 n_{A^*}}{\partial x^2} + \frac{D_{A^*}Q_A}{kT^2} \frac{dT}{dx} \frac{\partial n_{A^*}}{\partial x}. \quad (20)$$

The activation energy for self-diffusion is given by Q_A . The above parabolic partial differential equation with nonconstant coefficients cannot be solved exactly. The nonconstant coefficients arise from the fact that both the tracer diffusion coefficient and absolute temperature are functions of position.

The second term on the right-hand side of Eq. (20) causes a shift in the position of the maximum of the tracer profile toward the cold side, because, in a temperature gradient, the peak of the tracer profile is "eroded" away from the hot side where there is greater diffusion. This erosion would occur even if the velocity, V , of the lattice planes were zero.

An approximate solution to Eq. (20) can be obtained if it is assumed that D_{A^*} and $D_{A^*}Q_A/kT^2$ are constant. This is a reasonable approximation in the region near the lattice marker ($\leq 100 \mu$). For a temperature gradient of $300^\circ\text{C}/\text{cm}$ the maximum change in T is 0.3% and the maximum change in D is about 6% over this region. For an infinitesimally thin plane source, the approximate solution to Eq. (20) is

$$n_{A^*}(x,t) = \frac{n_0}{2[\pi D_{A^*}t + \pi D_{w^*}t]^{1/2}} \times \exp\left[-\frac{(x + V_1t - x_0)^2}{4D_{A^*}t + 4D_{w^*}t}\right]. \quad (21)$$

The effective anneal and weld times are t and t_w , respectively. D_w is the diffusion coefficient during welding, n_0 is the initial distribution of tracer, and x_0 is the location of the tracer peak at time $t=0$. Equation (21) satisfies Eq. (20) if $V_1 = (D_{A^*}Q_A/kT^2)dT/dx$. For the condition $\partial n_{A^*}/\partial x = 0$, the tracer profile maximum is located at the position satisfying the condition $x + V_1t - x_0 = 0$ at time t . The net shift of the tracer maximum is then

$$\Delta x_1 = -V_1t = (-D_{A^*}Q_A/kT^2)(dT/dx)t. \quad (22)$$

Far from the interface (~ 1 mm away) Eq. (21), which represents a shifted Gaussian, is not a good approximate solution to Eq. (20). The actual solution to Eq. (20) will be an asymmetric profile, but the peak will still be shifted by the amount given by Eq. (22), since the shifts are small ($\leq 50 \mu$) and (22) is an excellent approximation.

Experimentally, the initial interface was marked by immobile tracers fixed to the lattice frame of reference, and, since the lattice frame moves with respect to the laboratory frame, Eqs. (18) and (22) must be used together to obtain the shift of the peak of the tracer profile with respect to the marker. The total shift therefore is

$$\Delta x = -\frac{D_{A^*}}{kT^2} \left(Q_A + \frac{Q_{A^*} - \Delta H_F}{f} \right) \frac{dT}{dx} t. \quad (23)$$

The values of the temperature and diffusion coefficient that are used in Eq. (23) are calculated at a plane midway between the tracer profile maximum and the $\text{Hf}^{181}\text{O}_2$ lattice marker. These average values should be used in calculating finite shifts since, in fact, the velocities associated with the shifts are not constant but are also functions of x . Experimentally, the diffusion coefficient and temperature are measured at the peak of the tracer profile. The values at this position are only about 0.1 and 2% different from the average values for the temperature and diffusion coefficient, respectively.

B. Dilute Substitutional Impurity Thermomigration

Let A represent solvents atoms and B represent impurity tracer atoms. The general expressions for the flux of impurity tracer and solvent atoms in the lattice frame are⁴

$$J_A = D_A(\partial n_B/\partial x) - [L_{AA}(Q_A^* - \Delta H_F) + L_{AB}(Q_B^* - \Delta H_F)]T^{-2}dT/dx, \quad (24)$$

$$J_B = -D_B(\partial n_B/\partial x) - [L_{BA}(Q_A^* - \Delta H_F) + L_{BB}(Q_B^* - \Delta H_F)]T^{-2}dT/dx. \quad (25)$$

Here Q_A^* and Q_B^* are the heats of transport of solvent atoms and impurity tracer atoms, respectively.

The above equations were derived assuming that the vacancies were in local thermal equilibrium. For appreciable binding between the impurity and vacancy this would presumably only be an approximation because of the higher vacancy density around the impurity. Nevertheless, the approximation should be a good one for tracer amounts of impurity because the free vacancy concentration should be much larger than the impurity-vacancy pair concentration.

Since for tracer concentrations the solution is assumed to be ideal, the activity coefficient is independent of concentration, and D_A and D_B can be represented by

the following equations:

$$D_A = k[L_{AA}/n_A - L_{AB}/n_B], \quad (26)$$

$$D_B = k[L_{BB}/n_B - L_{BA}/n_A]. \quad (27)$$

Since $n_A \gg n_B$, one has $D_B \approx kL_{BB}/n_B$, where D_B is the tracer diffusion coefficient of the dilute impurity. For tracer concentrations, it can also be assumed that the influence of the solute impurity on the self-diffusion of the solvent atoms is negligible. In this case D_A is simply the self-diffusion coefficient of pure solvent atoms; $D_A = kL_{AA}/n_A$. Equations (24) and (25) therefore reduce to

$$J_A = +D_A \frac{\partial n_B}{\partial x} - \frac{n_A D_A}{kT^2} (Q_A^* - \Delta H_F) \frac{dT}{dx}, \quad (28)$$

$$J_B = -D_B \frac{\partial n_B}{\partial x} - \frac{n_B D_B}{kT^2} (Q_B^* - \Delta H_F) \frac{dT}{dx}. \quad (29)$$

The velocity of the lattice frame with respect to the laboratory frame is given by

$$nV = -(J_A + J_B), \quad (30)$$

where n is the concentration of lattice sites. Substitution of Eqs. (28) and (29) into Eq. (30) gives

$$V = \left(\frac{D_B - D_A}{n} \right) \frac{\partial n_B}{\partial x} + \frac{1}{nkT^2} [n_A D_A (Q_A^* - \Delta H_F) + n_B D_B (Q_B^* - \Delta H_F)] \frac{dT}{dx}. \quad (31)$$

The first term is the familiar Kirkendall shift and would be important for a nondilute binary alloy in a temperature gradient, but, under the present circumstances of a dilute alloy, this term is negligible compared to the second term. Since $n_A \approx n$ and $n_A \gg n_B$, (31) reduces to

$$V = (D_A/kT^2)(Q_A^* - \Delta H_F)(dT/dx). \quad (32)$$

This expression for the drift velocity is, of course, the same as that for the pure metal.

The flux of impurity tracer in the laboratory frame is given by

$$J_B^0 = J_B + n_B V. \quad (33)$$

Using the equations for J_B and V , J_B^0 becomes

$$J_B^0 = -D_B \frac{\partial n_B}{\partial x} - \frac{n_B}{kT^2} [D_B (Q_B^* - \Delta H_F) - D_A (Q_A^* - \Delta H_F)] \frac{dT}{dx}. \quad (34)$$

Substituting J_B^0 into the continuity equation for n_B gives

$$\frac{\partial n_B}{\partial t} = D_B \frac{\partial^2 n_B}{\partial x^2} + \frac{1}{kT^2} [D_B (Q_B + Q_B^* - \Delta H_F) - D_A (Q_A^* - \Delta H_F)] \frac{dT}{dx} \frac{\partial n_B}{\partial x}. \quad (35)$$

Q_B is the activation energy for the impurity atoms in the solvent matrix. The term proportional to n_B is negligible and has been neglected with respect to the other two terms on the right-hand side of Eq. (35). Again, near the interface ($\leq 100 \mu$), the diffusion coefficients and temperature will be approximately constant. The approximate solution to Eq. (35) is then

$$n_B(x,t) = \frac{n_0}{2[\pi D_B t + \pi D_w t_w]^{1/2}} \times \exp\left[-\frac{(x + V_1 t - x_0)^2}{4D_B t + 4D_w t_w}\right]. \quad (36)$$

The shift of the tracer profile maximum with respect to the laboratory marker is

$$\Delta x_1 = -V_1 t = -\frac{1}{kT^2} [D_B (Q_B + Q_B^* - \Delta H_F) - D_A (Q_A^* - \Delta H_F)] \frac{dT}{dx} t. \quad (37)$$

This equation is seen to be somewhat more complicated than Eq. (22) which represents the shift for tracer self-thermomigration with respect to a laboratory marker.

The shift of the two reference frames for an anneal time t is obtained from Eq. (32)

$$\Delta x_2 = -\frac{D_A}{kT^2} (Q_A^* - \Delta H_F) \frac{dT}{dx} t. \quad (38)$$

Therefore, the shift of the tracer profile maximum with respect to the lattice marker is

$$\Delta x = -\frac{D_B}{kT^2} (Q_B + Q_B^* - \Delta H_F) \frac{dT}{dx} t. \quad (39)$$

The second term in Eq. (37) due to the shift of solvent atoms cancels exactly.

Again, average values of the diffusion coefficient and temperature, calculated at a plane midway between the tracer profile maximum and the Hf¹⁸¹O₂ lattice marker, are used to calculate the effective heat of transport $Q_B + Q_B^* - \Delta H_F$.

III. EXPERIMENTAL PROCEDURE

A. Specimen Fabrication and Radioactive Isotope Application

The Au used in this experiment was purchased from Handy and Harmon Corporation in the form of polycrystalline rods (99.95% pure) $\frac{1}{4}$ in. in diameter. The rods were turned to a $\frac{3}{16}$ -in. diam on a lathe, cut to the appropriate length, and then threaded at both ends with a 10-32 dye. Each specimen was then spark cut perpendicular to the long axis at two parallel faces separated by $\frac{1}{8}$ in., and the four cut surfaces were then

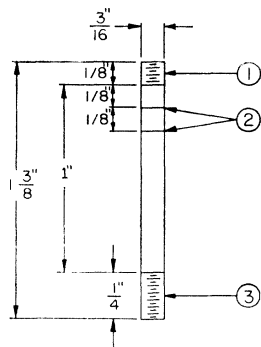


FIG. 1. Schematic of a specimen: 1, threaded end which screws into hot junction; 2, welded interfaces containing tracer and inert $\text{Hf}^{181}\text{O}_2$ marker; and 3, threaded end which screws into cold junction.

lapped optically flat. A schematic of a typical specimen is shown in Fig. 1.

A thin uniform layer of radioactive tracer was deposited on each face of the $\frac{1}{8}$ -in. high disk. A count rate between 50 000 and 150 000 counts/min was obtained for all isotope layers. The Au^{195} and Sb^{125} radioactive isotopes were obtained from Nuclear Science and Engineering Corporation. The Hf^{181} isotope was obtained from Oak Ridge National Laboratory. All isotopes were received in approximately 0.5 *N* HCl solutions. The 185-day Au^{195} and 3-yr Sb^{125} isotopes were applied by simply drying the solutions onto the optical flats. Both AuCl_3 and SbCl_3 dissociate at temperatures much lower than the welding temperature so that the dissociation was complete in the final welded specimen. Since the specimens were only 0.187 in. in diameter, only a small side cut was permitted. Thus radioactive contamination on the side of the specimen was intolerable. For this reason drying of the radioactive isotope onto the face of the specimen was chosen instead of electroplating since no adequate side mask was found that satisfied the requirement for complete masking without contaminating the plating bath.

The 45-day Hf^{181} was also dried onto the two mating surfaces adjacent to the surfaces deposited with radioactive tracer. The Hf^{181} was in the chemical form HfOCl_2 and was oxidized using concentrated HNO_3 . The resulting nondiffusing radioactive HfO_2 with a very high dissociation temperature served to mark the lattice interface.

B. Welding Apparatus

The next step in the procedure was to reassemble the specimen for welding. A special stainless steel brace was fabricated to support the specimen for mounting in the welding rig. It was possible to line up all three pieces of the specimen with no overlap of edges using this brace. The assembled specimen and brace were then inserted into the molybdenum welding apparatus which is shown in Fig. 2. As seen in the figure, the specimen alignment pieces touched the molybdenum body in two adjacent rings with a clearance of approximately 1 mil. This was necessary to keep the alignment pieces from welding to the body of the welding apparatus at the

welding temperature. The tightening screws touched the alignment pieces at only one point to keep the alignment pieces straight during welding. After the specimen had been inserted into the welding apparatus the stainless steel brace was removed through one of the three viewing ports. The specimen touched the welding apparatus only at each end, separated by a thin piece of mica to keep the specimen from welding to the alignment pieces. The assembled molybdenum welding apparatus and specimen were then placed in a vertical-tube vacuum furnace. A thermocouple was inserted at a viewing port to monitor the temperature of the specimen. At the welding temperature the specimen was under pressure due to the difference in thermal expansion of the Au specimens and the molybdenum welding rig. The welding temperature was approximately 950°C , which is 113°C under the melting point of Au. The effective welding time was on the order of an hour. The radioactive tracer penetration was between 50 and $100\ \mu$ during the weld. This amounted to approximately 3% of the total penetration after the temperature gradient anneal for the tracer at the hot interface and approximately 10% for the tracer at the cold interface. During the welding anneal the length of the specimen decreased by approximately $\frac{1}{2}\%$. This was, of course, expected since uniaxial pressure was required to effect the welds.

All weld attempts were successful. Examination of the welds indicated that they were sound, and this visual observation was corroborated by subsequent lathe sectioning. After the specimen was welded, a small hole approximately 30 mils in diameter and 30 mils deep was drilled into the top of the specimen. The control thermocouple was inserted into this well during the diffusion anneal and actually welded to the specimen.

C. Thermomigration Apparatus

The welded specimen was then placed into the temperature gradient furnace for the diffusion anneal. A schematic of the furnace is shown in Fig. 3. During

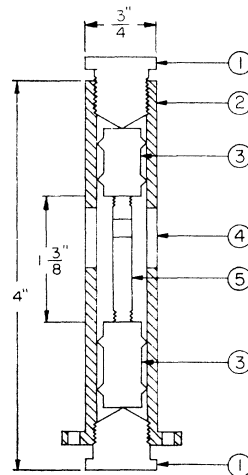


FIG. 2. Assembled molybdenum welding apparatus with specimen: 1, tightening screws; 2, apparatus body; 3, specimen alignment pieces; 4, viewing port; and 5, specimen.

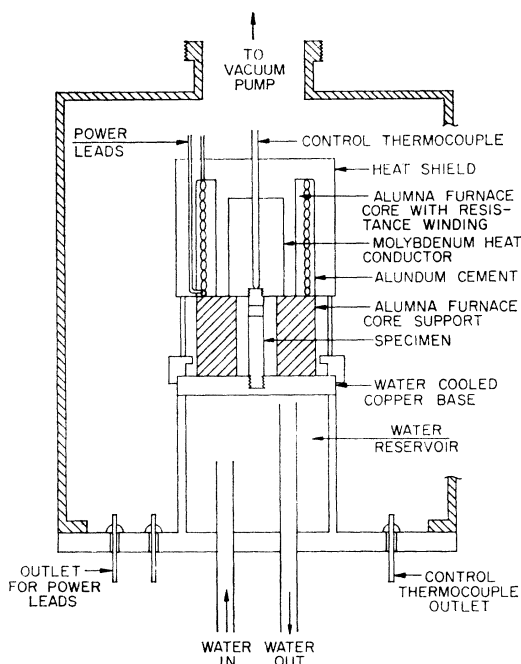


FIG. 3. Schematic of temperature gradient furnace.

the runs the specimen was cooled at one end by screwing it into a water-cooled copper base, and it was heated at the other end by screwing it directly into a molybdenum heat conductor. A control thermocouple was inserted in a hole along the cylindrical axis of the heat conductor to contact the top of the specimen; this couple controlled the temperature of the specimen at its hottest point. No thermocouples which might possibly adversely affect the temperature gradient by acting as heat sinks were inserted along the specimen length. The specimen was allowed to expand freely upward when heated, since only the threaded portion was actually in physical contact with the molybdenum heat conductor. The distance between the welds was measured before and after the diffusion anneal, and no change could be detected using a microscope capable of measuring distances accurate to 0.1 mil.

A dynamic vacuum of 10^{-5} mm was maintained within the chamber to reduce conduction and convection losses and also to preserve the life of the molybdenum furnace winding. The heat radiation shield consisted of two concentric tantalum cylinders. An input power of approximately 600 W was necessary to provide a temperature gradient of nearly $800^{\circ}\text{C}/\text{in}$. About half of this power was necessary to provide the temperature gradient and the remainder to compensate other heat losses. The entire furnace assembly was separated thermally from the water-cooled copper base by ceramic support insulators. This was necessary to keep the input power to a minimum. Even with as much insulation as possible the temperature at the molybdenum furnace winding was estimated to be in excess of 1300°C to

maintain a temperature of 1040°C at the top of the gold specimen.

The temperature at the top of the Au specimens was maintained to within $\pm 1^{\circ}\text{C}$ at 1040°C for periods up to two weeks using a Thermac Solid-State Temperature Controller. The temperature at the water reservoir was monitored periodically and found to be within $\pm \frac{1}{2}^{\circ}\text{C}$ at approximately 20°C .

D. Sectioning Procedure

During the diffusion anneal the control thermocouple and molybdenum heat conductor welded to the top of the Au specimens. After removal from the furnace, the specimen was cut off at an appropriate distance below the second weld. The molybdenum heat conductor was then mounted in the lathe and the attached specimen was aligned prior to sectioning. Using a special adjustable chuck, it was possible to align the cylindrical axis of the specimen to within 0.02 rad of the lathe axis, and both weld planes could be lined up perpendicular to the lathe axis. Mechanical support of the $\frac{3}{16}$ -in. diam specimens was not necessary since the sandwich welds proved strong enough to withstand the applied cutting tool stresses. The total distances sectioned at the hot and cold interfaces were 2 to 3 mm and 1 mm, respectively. Since the average section thickness far from the interface was $12\ \mu$, many sections were required for each interface. Close to the HfO_2 interface approximately $4\ \mu$ sections were taken. If smaller sections were attempted, the tool usually rubbed against the surface and poor cuts resulted. The number of sections taken for each interface was usually between 50 and 100. A water-soluble lubricant was used as a cutting aid because the Au chips had a tendency to weld back to the face if the chips were cut dry. The chip plus lubricant was placed on filter paper and saturated with ethyl alcohol. Most of the lubricant was absorbed by the filter paper; the remainder was burned away using an infrared lamp. This procedure for removing the lubricant was tested on a dummy specimen and found to be completely effective.

E. Weighing and Counting Procedure

The chips were weighed using a Mettler semimicro balance. The average chip weight was about 8 mg with an error of ± 0.02 mg, giving an error between $\frac{1}{4}$ and $\frac{1}{2}\%$ in section weights. All radioactivities were assayed using a conventional γ -ray scintillation system. The Au^{195} distribution was determined using a window corresponding to the $\text{Au}^{195} K$ x ray; the Sb^{125} distribution was determined by counting its two highest-energy γ rays, and the Hf^{181} distribution was determined using its highest-energy γ rays. At least 10 000 counts were taken for each chip, giving a percent error of no more than 1% for the count rate. The specific activity, which is the count rate divided by the chip weight, was thus accurate to approximately 1.1%. The penetration distance was determined by directly adding the chip

weights, thereby avoiding error due to tool wear or dial-gauge slippage.

IV. EXPERIMENTAL RESULTS

A. Method Used to Curve Fit Tracer Profiles

From the previous derivation, the concentrations n_{A^*} of tracer solvent atoms and n_B of tracer solute atoms are given by

$$\frac{\partial n_{A^*}}{\partial t} = D_{A^*} \frac{\partial^2 n_{A^*}}{\partial x^2} + \frac{D_{A^*} Q_A}{kT^2} \frac{dT}{dx} \frac{\partial n_{A^*}}{\partial x},$$

$$\frac{\partial n_B}{\partial t} = D_B \frac{\partial^2 n_B}{\partial x^2} + \frac{[D_B(Q_B + Q_B^* - \Delta H_F) - D_A(Q_A^* - \Delta H_F)]}{kT^2} \frac{dT}{dx} \frac{\partial n_B}{\partial x}.$$

Since these equations have nonconstant coefficients, it is not possible to solve them exactly over the 1 to 3 mm range in x of the tracer spread, inasmuch as the diffusion coefficients and absolute temperatures vary considerably over this range.

Therefore, the following method was used for solution: Since the solutions to these equations for constant coefficients are just Gaussians in x [the solutions are given by Eqs. (21) and (36)] centered at the extremum positions, a plot of the natural logarithm of the concentration versus x for these solutions is obviously a polynomial in x of order 2. Thus it seemed reasonable to suppose that for a nonzero temperature gradient a plot of the natural logarithm of the experimental tracer concentration could be fit by the method of least squares by a general polynomial in x of order 2 or higher, depending on the skewness and range of the profile. This method was tried and proved to be very successful. An IBM 7094 computer program was used to fit the experimental log concentrations versus x values with polynomials in x from orders 2 through 8. The best fit curve was chosen on the basis of the minimum standard deviations of the polynomial coefficients and the maximum number of experimental points which fell within

one standard deviation. On this basis all curves were best fit with a polynomial of order 3 except in two cases. In one case, which was order 2 fit, the range of x was about 300 μ ; this verifies experimentally that for a small range of x it is correct to use the constant coefficient solutions. In the other case, which was an order 4 fit, the range of x was about 3300 μ ; this order of fit is entirely reasonable since the range was very large. Actually, the rejected fits of orders 4 and 5 gave the same profile maximum to within a few microns, indicating that the position of the profile maximum given by the least squares fit is essentially independent of the details of the fit.

For the best fit curves the error in the polynomial coefficients was usually between 1 and 2%, and the percentage of experimental points falling within one standard deviation was around 70%. Table I gives a summary of the percentage of data points within one standard deviation for all runs.

B. Interface Temperature Measurement and Calculation of Dt Values

As mentioned in Sec. III, no monitoring thermocouples were placed in contact with a specimen during an anneal because of the possibility of disturbing the linear temperature gradient and the radioactive tracer profile. It might have been possible to approximate the interface temperature by measuring the temperature at each end of the specimen and assuming a linear gradient over the length of the specimen. This method has been used by earlier investigators to determine the temperature at a given point in self-thermomigration experiments. However, it will be shown below that this method of estimating temperature can introduce large errors in the calculated values for the heat of transport.

In all self-thermomigration experiments the measured shifts are proportional to the diffusion coefficients. Most shift expressions are of the form

$$\Delta x = (Dt/kT^2)(dT/dx)Q^{**}; \quad (40)$$

Q^{**} is an effective heat of transport, Δx is the measured shift, and D is the diffusion coefficient. Since the diffusion coefficient $D = D_0 \exp(-Q/kT)$, an error in T is related to an error in D by the relation

$$\Delta D/D = Q/kT(\Delta T/T). \quad (41)$$

If the interface temperature cannot be measured directly, it is difficult to estimate the temperature by interpolation to better than $\pm(10-20)^\circ\text{C}$ at a diffusion temperature of 1000°K; the percent error in T is then 1-2%. But since Q/kT is of the order of 20, by Eq. (41) this gives an error in D of 20-40%. From Eq. (40) this makes Q^{**} uncertain by the uncertainty in D .

A far more precise method for measuring the temperature at the diffusion interface can be used in the present experiment. From the measured values for the diffusion coefficients determined from the experimental

TABLE I. A summary of the percentage of data points within one standard deviation for all runs.

Run Number	Radioactive tracer	Interface	Total number of points	Order of fit	Percentage of points within one std. dev.
1	Au ¹⁹⁵	cold	56	3	80
1	Au ¹⁹⁵	hot	66	3	74
2	Au ¹⁹⁵	cold	66	3	85
2	Au ¹⁹⁵	hot	98	4	77
3	Au ¹⁹⁵	cold	25	2	70
3	Sb ¹²⁵	cold	46	3	78
3	Au ¹⁹⁵	hot	22	3	68
3	Sb ¹²⁵	hot	63	3	71

TABLE II. Summary of the polynomial coefficients for the best fit curve in X^n of the logarithm of specific activity of Au¹⁹⁵ in Au for runs 1 and 2.

Run no.	Interface	Order of fit	A_0	$A_1(10^2 \text{ cm}^{-1})$	$A_2(10^3 \text{ cm}^{-2})$	$A_3(10^3 \text{ cm}^{-3})$	$A_4(10^3 \text{ cm}^{-4})$
1	cold	3	6.026±0.031	3.456±0.030	-5.044 ±0.080	13.94±0.63	
1	hot	3	6.869±0.015	1.381±0.007	-1.049 ±0.008	1.646±0.030	
2	cold	3	5.778±0.031	2.815±0.017	-2.566 ±0.026	4.190±0.120	
2	hot	4	5.765±0.015	1.445±0.006	-0.8372±0.0079	1.628±0.038	-1.300±0.062

TABLE III. Summary of polynomial coefficients for the best fit curve of the logarithm of specific activity of Au¹⁹⁵ and Sb¹²⁵ in Au for run 3.

Radioactive tracer	Interface	Order of fit	A_0	$A_1(10^2 \text{ cm}^{-1})$	$A_2(10^3 \text{ cm}^{-2})$	$A_3(10^3 \text{ cm}^{-3})$
Au ¹⁹⁵	cold	2	-54.72 ±0.83	22.12 ±0.27	-17.70 ±0.21	
Sb ¹²⁵	cold	3	6.165±0.034	1.674 ±0.019	-1.661 ±0.031	3.393 ±0.150
Au ¹⁹⁵	hot	3	-73.60 ±1.50	18.24 ±0.38	-12.02 ±0.32	23.87 ±0.87
Sb ¹²⁵	hot	3	6.018±0.022	0.9008±0.0063	-0.4875±0.0050	0.6558±0.0112

tracer profiles, and from the known values of D_0 and Q for self-diffusion, the temperatures at the interfaces could be calculated using the equation $D = D_0 e^{-Q/kT}$. In the present experiment, most diffusion coefficients were accurate to about 5%; thus T could be determined to about 1/4%. It is important to stress that in this experiment the Dt values were determined directly from the experimental data and did not have to be calculated

from separate temperature measurements; thus Dt in each case was known within about 5%.

The Dt calculations were made as follows: For an initial instantaneous plane source at $x = x_0$ and at a constant temperature T , the natural logarithm of the concentration at time t is given by

$$\ln n = \text{const} - [(x - x_0)^2 / (4Dt + 4D_w t_w)] = A_0 + A_1 x + A_2 x^2. \quad (42)$$

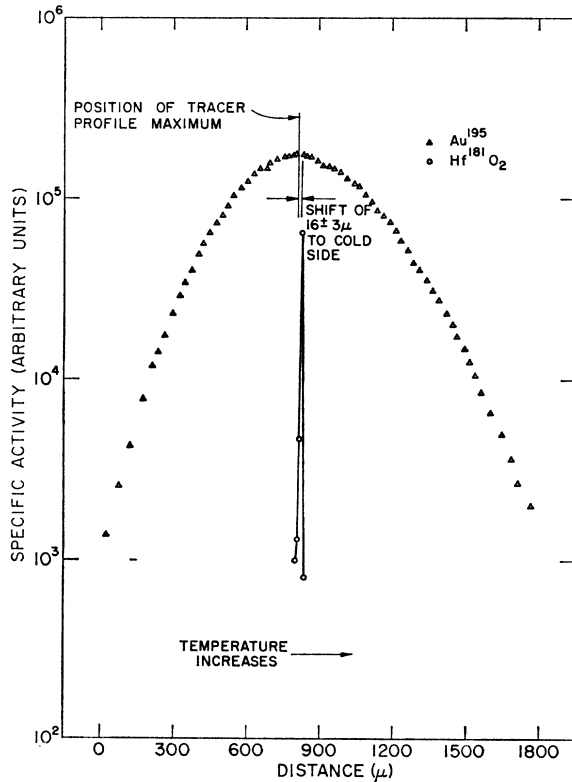


FIG. 4. Distribution of Au¹⁹⁵ tracer and Hf¹⁸¹O₂ marker at the hot interface in run 1.

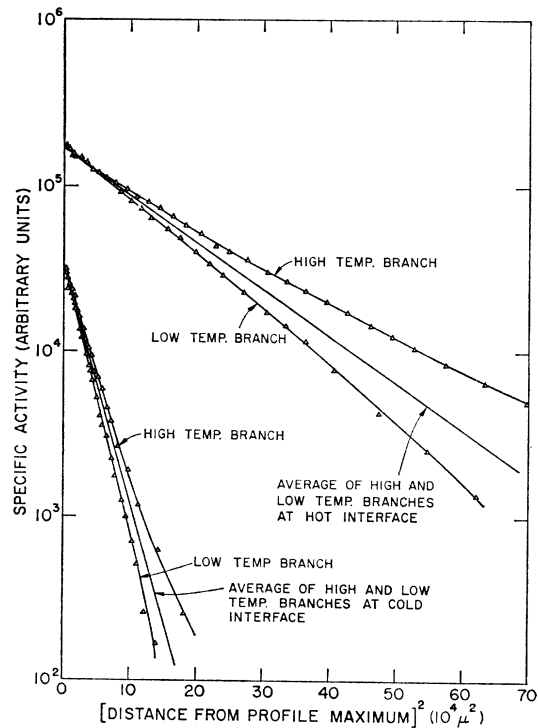


FIG. 5. Au¹⁹⁵ penetration profiles at the hot and cold interfaces in run 1.

The coefficient A_2 is proportional to the second derivative of

$$\partial^2 \ln n / \partial x^2 = 2A_2 = -2(4Dt + 4D_w t_w)^{-1}. \quad (43)$$

The best fit curves in polynomials of order 3 for the asymmetric Gaussians can be represented by the equation

$$\ln n = A_0 + A_1 x + A_2 x^2 + A_3 x^3. \quad (44)$$

Therefore,

$$\frac{\partial^2 \ln n}{\partial x^2} = 2A_2 + 6A_3 \bar{x}. \quad (45)$$

Since the Dt values are calculated at the extremum position, \bar{x} in Eq. (45) is the extremum. Using Eq. (43) as the definition of the slope and also Eq. (45) gives

$$-(4Dt + 4D_w t_w)^{-1} = A_2 + 3A_3 \bar{x}. \quad (46)$$

Since $A_2 + 3A_3 \bar{x} = -(A_2^2 - 3A_1 A_3)^{1/2}$, Eq. (46) becomes

$$(4Dt + 4D_w t_w)^{-1} = (A_2^2 - 3A_1 A_3)^{1/2}. \quad (47)$$

Equation (47) was used to calculate the Dt values at the tracer peak using the best fit values A_1, A_2, A_3 , and the welding correction $D_w t_w$. Tables II and III give the best fit polynomial coefficients for runs 1 and 2 for Au^{195} self-thermomigration and run 3 for Sb^{125} dilute impurity thermomigration in Au, respectively. The

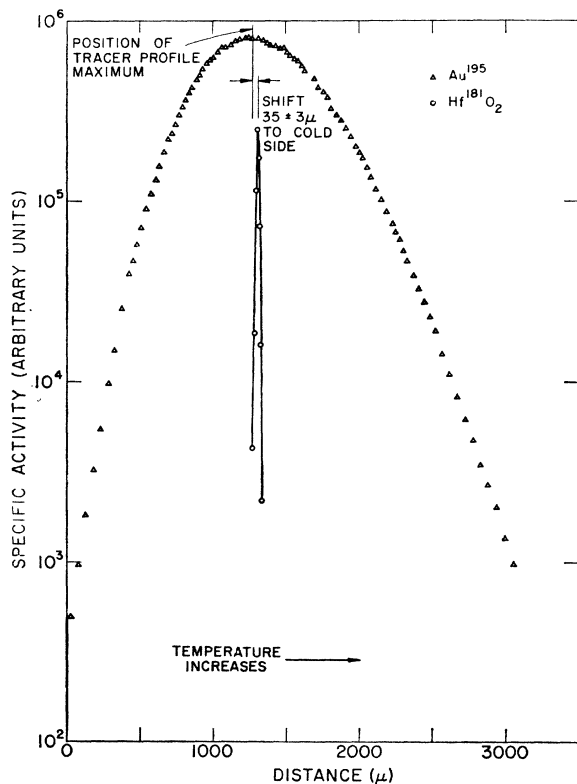


Fig. 6. Distribution of Au^{195} tracer and $\text{Hf}^{181}\text{O}_2$ marker at the hot interface in run 2.

tracer diffusion coefficient of Au^{195} in Au has been measured by Gilder and Lazarus²⁰ who obtained $D_0 = 0.107 \text{ cm}^2 \text{ sec}^{-1}$ and $Q = 1.83 \text{ eV}$. This measurement was used to calculate the temperature at the profile maximum to $\frac{1}{4}\%$.

The temperature gradient was calculated by using the calculated values of temperature at the hot and cold interfaces of a given specimen and the measured distance between them. The temperature gradients were thus accurate to about 4%. The only purpose of the cold interface was to measure the temperature at another point along the specimen so that an accurate determination of the temperature gradient could be made.

C. Shift of Au Tracer

Two tracer self-thermomigration runs were performed in Au using Au^{195} . Figure 4 shows the distribution of the Au^{195} at the hot interface in run 1. A shift of $-16 \pm 3 \mu$ was measured. The largest source of error in the shift measurement is the location of the $\text{Hf}^{181}\text{O}_2$ layer. This was done to within about $\pm 2 \mu$ by taking very small cuts through the interface. Figure 5 is a plot of the Au^{195} penetration profiles versus distance from the profile maximum squared in run 1. The skewness of the

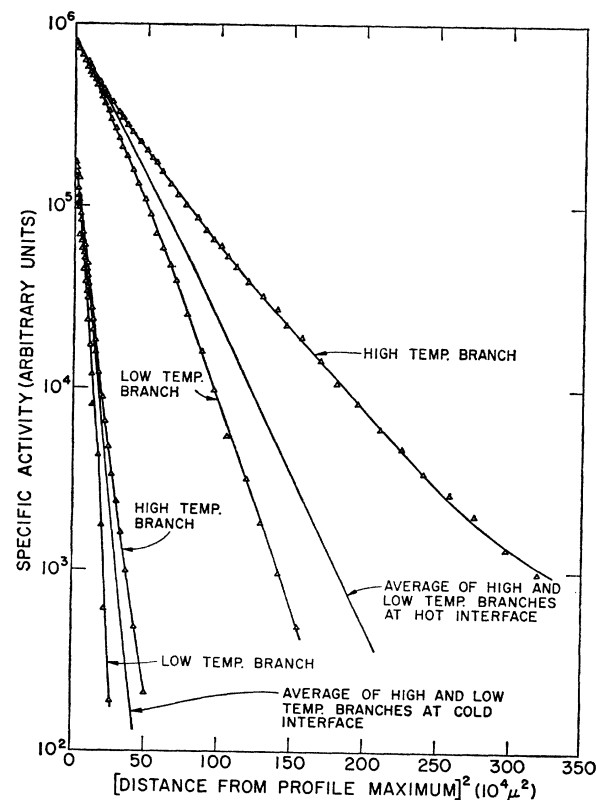


Fig. 7. Au^{195} penetration profiles at the hot and cold interfaces in run 2.

²⁰ H. M. Gilder and D. Lazarus, J. Phys. Chem. Solids 26, 2081 (1966).

profiles due to the temperature gradient is clearly evident from this figure. The average of the high- and low-temperature branches was obtained by reflecting the low-temperature branch of a given profile about the extremum to the high-temperature side and averaging with the high-temperature branch; the slope of the plot of the average of the two branches versus $(x-\bar{x})^2$ also gives the Dt values at the tracer peak.

Figures 6 and 7 show similar results for the Au¹⁹⁵ distributions in run 2. The range of x is larger than for run 1. A shift of $-35 \pm 3 \mu$ was measured at the hot interface.

D. Shift of Sb Tracer

The diffusion coefficient of Sb¹²⁵ has not been previously measured in Au. Thus it was necessary to diffuse both Au¹⁹⁵ and Sb¹²⁵ together in Au to establish an accurate temperature scale. The Sb¹²⁵ Dt values were determined from the Sb tracer profiles. The temperature at the Sb profiles was determined from the Au Dt values and the known diffusion coefficient of Au¹⁹⁵ in Au. Figures 8 and 9 show the Sb¹²⁵ and Au¹⁹⁵ tracer distributions at the cold and hot interfaces, respectively. An Sb¹²⁵ tracer profile shift of $+51 \pm 3 \mu$ was measured at the hot interface. In this run it was actually possible to separate the hot interface with the lathe cutting tool at a distance of a few microns away. This was probably

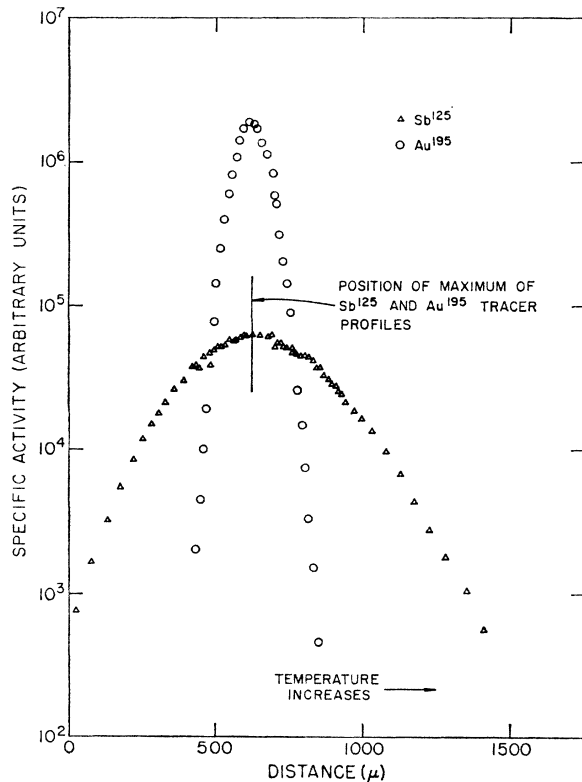


FIG. 8. Distribution of Sb¹²⁵ and Au¹⁹⁵ tracers at the cold interface in run 3.

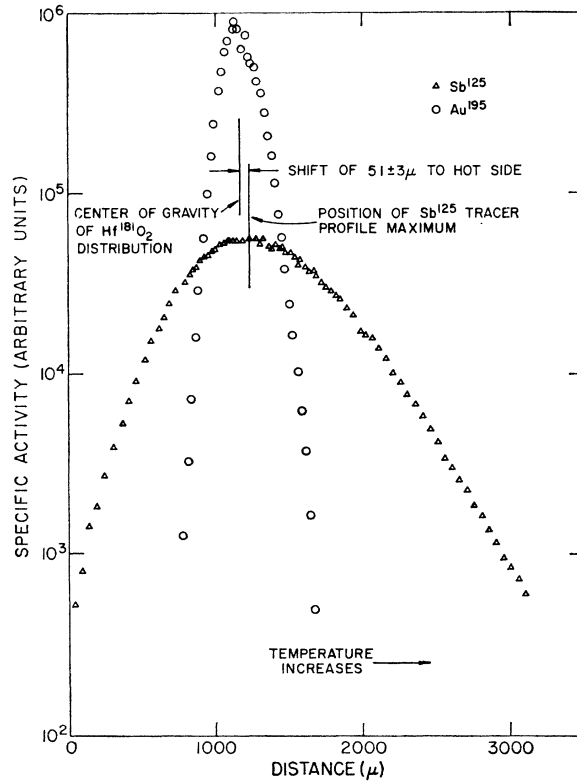


FIG. 9. Distribution of Sb¹²⁵ and Au¹⁹⁵ tracers at the hot interface in run 3.

possible because the diffusion time for this run was 1 day whereas the diffusion time for runs 1 and 2 was about 10 days, all at about the same temperature; welding was therefore probably less complete. Figures 10 and 11 are plots of the Au¹⁹⁵ and Sb¹²⁵ penetration profiles versus distance from the extremum squared, respectively, in run 3.

V. DISCUSSION OF RESULTS AND CONCLUSIONS

A. Comparison of Self-Thermomigration Results with Theory

Table IV includes all the measured and calculated parameters for runs 1 and 2 for tracer self-thermomigration in Au. Eq. (23) was used to calculate the effective heat of transport $Q_{Au} + (Q_{Au}^* - \Delta H_F)/f$ of the Au atoms. The temperature gradients for the two runs agree almost exactly within experimental error, indicating that the specimens were annealed under nearly identical conditions. The major difference in the effective heats of transport is attributable to errors in locating the Hf¹⁸¹O₂ layer. The average value of the effective heat of transport $Q_{Au} + (Q_{Au}^* - \Delta H_F)/f$ is 1.60 ± 0.27 eV. With $Q_{Au} = 1.83$ eV for the activation energy for diffusion of Au¹⁹⁵ in Au,²⁰ $\Delta H_F = 0.98$ eV for the Au

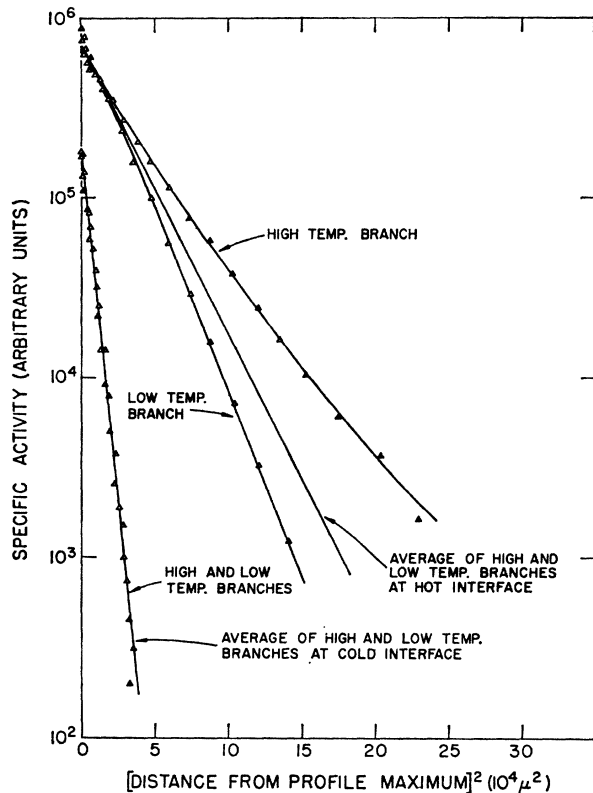


FIG. 10. Au¹⁹⁶ penetration profiles at the hot and cold interfaces in run 3.

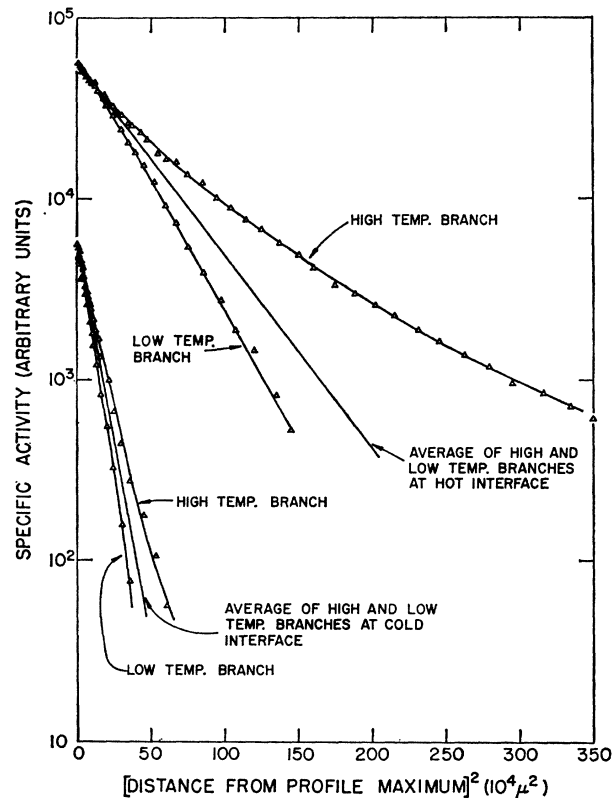


FIG. 11. Sb¹²⁵ penetration profiles at the hot and cold interfaces in run 3.

vacancy formation energy,²¹ and $f=0.78$ for the fcc lattice,¹⁹ the heat of transport is found to be $Q_{Au}^* = 0.80 \pm 0.27$ eV.

The motion energy of Au atoms²¹ has been measured to be $\Delta H_M = 0.82 \pm 0.05$ eV. Comparing the measured value of the heat of transport with the motion energy indicates excellent agreement with Huntington's theory for single-band metals. Apparently, as predicted, the contribution to the heat of transport from the static temperature gradient far outweighs the contributions from the thermoelectric field and charge carrier-ion interaction. Thus, the diffusing atom carries almost all of its migration energy with it when jumping from a given site to an adjacent vacant site.

The presently measured value of $Q_{Au}^* = 0.80$ eV can be compared with the three previous measurements in which scratch marks and internal wires were used. Adda *et al.*⁷ obtained $Q_{Au}^* \approx \Delta H_F = 0.98$ eV using the internal wire technique; Meechan and Lehman⁶ using the internal wire technique obtained $Q_{Au}^* \approx 0.8$ eV for one run, and larger values for their other two runs; and Jaffe and Shewmon⁵ obtained $Q_{Au}^* \approx 0.6$ eV using the scratch mark technique. For reasons noted earlier, the present result is hopefully more accurate than any of the values reported previously.

²¹ R. O. Simmons, J. S. Koehler, and R. W. Bulluffi, *Radiation Damage Solids* 1, 155 (1962).

B. Comparison of the Sb Impurity Thermomigration Result with Theory

Table V includes all the measured and calculated parameters for run 3 for Sb¹²⁵ impurity thermomigration in Au. Equation (39) was used to calculate the effective heat of transport $Q_{Sb} + Q_{Sb}^* - \Delta H_F$ of the impurity Sb atoms. This value is -1.61 ± 0.16 eV. Q_{Sb} is the Sb diffusional activation energy in Au. It was possible to measure Q_{Sb} directly in this experiment because D values for Sb¹²⁵ in Au were measured at two positions in the rod and the temperature at these positions was measured using the Au¹⁹⁴ tracer. Q_{Sb} was measured to be 1.39 ± 0.17 eV. Gilder and Lazarus²² estimated a value of 1.2 eV for this parameter on the basis of two points while studying electromigration of Sb¹²⁵ in Au. A value of $Q_{Sb} = 1.39$ eV compares favorably with the measured activation energy for diffusion of Sb in Ag²³ which is 1.67 eV. Using $Q_{Sb} = 1.39$ eV and $\Delta H_F = 0.98$ eV (the vacancy formation energy adjacent to a solute atom is assumed to be equal to the formation energy in the pure metal) gives $Q_{Sb}^* = -2.02 \pm 0.23$ eV. This large negative heat of transport indicates that there is a net flux of Sb atoms up the temperature gradient in

²² H. M. Gilder and D. Lazarus, *Phys. Rev.* 145, 507 (1966).

²³ E. Sonder, L. Slifkin and C. T. Tomizuka, *Phys. Rev.* 93, 970 (1954).

TABLE IV. Parameters describing the thermomigration of Au¹⁹⁵ in Au for runs 1 and 2.

Run no.	Interface	Time (10 ⁵ sec)	Diff. coeff. (10 ⁻¹⁰ cm ² sec ⁻¹)	Temp. (°C)	Temp. grad. (°C cm ⁻¹)	Shift (μ)	Q+(Q*-ΔH _F)/f (eV)
1	cold	7.52	0.854±0.005	741±3			
1	hot	7.52	4.98 ±0.13	834±2	315±12	-16±3	1.43±0.27
2	cold	8.50	1.56 ±0.05	771±2			
2	hot	8.50	8.47 ±0.44	867±3	309±12	-35±3	1.76±0.18

Au. Biermann *et al.*²⁴ investigated the heat of transport of Sb in Ag by measuring the thermal gradient redistribution of Sb in Ag under steady state conditions, and found $Q^*_{\text{Sb}} - \Delta H_F = -1.47 \pm 0.27$ eV. This value can be compared with the present calculated value for Sb in Au; $Q^*_{\text{Sb}} - \Delta H_F = -3.00 \pm 0.23$ eV. The values compare favorably and indicate that basically the same interactions are taking place in both Au and Ag.

The present result indicates, according to Huntington's theory, that the electron-impurity ion interaction is very large (as might be expected, since the valence difference between Sb and Au is +4) and drives the Sb atoms toward the hot end of the specimen. This means that the cold electrons moving up the temperature gradient deliver more momentum to the impurity atoms than the hot electrons moving down the temperature gradient. This can only be possible if the scattering cross section of the impurity by the electrons is a decreasing function of energy. Gerl¹³ has investigated theoretically the effect of the temperature gradient on impurity atoms in great detail. His expression for the force acting on an impurity atom (which is proportional to the negative of the heat of transport contribution of the heat carrier-impurity ion interaction) is

$$\frac{F_z}{|\nabla T|} = -M A_z(E_F) \left(1 + 2 \frac{dA/A}{dE/E} \right)_{E_F} \quad (48)$$

M is a characteristic of the matrix, $A_z(E_F)$ is the scattering cross section of the impurity ion, evaluated at the Fermi energy, and $[(dA/A)/(dE/E)]_{E_F}$ represents the change in the scattering cross section with electron energy evaluated at the Fermi energy. The

present experimental result would indicate that the enclosed term on the right in Eq. (48) is negative. Gerl also derived a more complicated expression for Eq. (48), taking into account the scattering effect of the neighboring vacancy of the impurity atom. From known thermoelectric power data, the contribution to the heat of transport due to the electron-antimony ion interaction in Ag at 900°C was calculated to be $Q^* = -0.5$ eV. A similar calculation was not made for Sb in Au, but the theoretical result in Ag does indicate that there could be a large negative heat of transport contribution in Au due to the electron-impurity ion interaction, in agreement with the present result.

A final point should be made concerning the impurity thermomigration. The situation for appreciable binding between a vacancy and impurity atom may differ from that for a weakly bound impurity. In the present experiment because Sb diffuses some 10 times faster than Au it is expected that a majority of the Sb atoms would be bound to vacancies. The effect of the temperature gradient on the ω_1 solvent-vacancy jumps of the associated vacancy would probably affect the motion of the Sb-vacancy complex. Using the kinetic theory, an expression can be derived for the effective heat of transport of the impurity atom, $Q^*_{B} - \Delta H_F$, which involves added parameters to account for this association. According to the model of Howard and Manning²⁵, for tight binding, the effective heat of transport $Q^*_{B} - \Delta H_F = q_2^* - 2q_1^* + (1-p)\Delta H_F$; p is the fraction of associated impurity atoms, q_2^* is the heat of transport corresponding to the impurity atom-vacancy exchange (ω_2 jumps), and q_1^* is the heat of transport corresponding to the associated vacancy exchanging with a

TABLE V. Parameters describing the thermomigration of Sb¹²⁵ in Au for run 3.

Radioactive tracer	Interface	Time (10 ⁴ sec)	Diff. coeff. (10 ⁻¹⁰ cm ² sec ⁻¹)	Temp. (°C)	Temp. grad. (°C cm ⁻¹)	Shift (μ)	Q+Q*-ΔH _F (eV)
Au ¹⁹⁵	cold	9.80	0.797±0.073	738±4			
Sb ¹²⁵	cold	9.80	20.9 ±2.1				
Au ¹⁹⁵	hot	9.80	6.20 ±0.12	848±2			
Sb ¹²⁵	hot	9.80	100.9 ±7.3		347±14	51±3	-1.61±0.16

²⁴ W. Biermann, D. Heitkamp, and T. S. Lundy, *Acta Met.* 13, 71 (1965).

²⁵ R. E. Howard and J. R. Manning, *J. Chem. Phys.* 36, 910 (1962).

solvent atom (ω_1 jumps). For the present case, assuming $p \approx 1$ and $q_1^* \approx Q_{Au}^* = 0.80$ eV and taking $Q_{Sb}^* - \Delta H_F = -3.00$ eV implies that $q_2^* \approx -1.40$ eV for the heat of transport associated with the ω_2 jumps alone, in somewhat closer agreement with Gerl's predicted value for Sb in Ag.

ACKNOWLEDGMENTS

The author wishes to thank his advisor, Professor David Lazarus, for his guidance and encouragement throughout this research. Also, he would like to thank Dr. W. D. Seward and Dr. D. Gupta for helpful discussions.

Effect of Hydrostatic Pressure on the Recovery of Electrical Properties of Neutron-Irradiated Molybdenum†

G. L. KULCINSKI

Battelle Memorial Institute, Pacific Northwest Laboratory, Richland, Washington 99352

(Received 14 October 1968)

High-purity molybdenum has been irradiated at 40°C to a fluence of 6.2×10^{18} n/cm² ($E > 1$ MeV) and subsequently isochronally annealed at two pressures, ≤ 1 and 20 000 bar. At low pressure, the electrical resistance increase recovers in three stages, at 150, 425, and 575°C. The effect of pressure is to lower the 150°C recovery peak to 90°C; this shift implies a negative activation volume of migration of -0.9 molar volumes for the migrating defect. The 425°C peak is apparently also lowered by pressure, but because of its small magnitude and uncertainty in its position, more detailed data are required before any pressure coefficient can be determined. The final 575°C recovery peak is lowered to 375°C under pressure and displays a pressure coefficient of $-10^\circ\text{C}/\text{kbar}$.

I. INTRODUCTION

THE recovery of irradiation-produced defects in molybdenum has been studied by many investigators with particular attention being paid to stage-III recovery at $\sim 150^\circ\text{C}$. Unfortunately, there still is no general agreement on the species migrating in stage III, and the interpretations of the data usually fall into one of two camps. The first group¹⁻⁵ feels that interstitials, either free or those released from traps, are migrating to immobile vacancies or adding on to interstitial clusters. The second group⁶⁻¹¹ feels that vacancies

are migrating to trapped interstitials, to interstitial clusters, or to small vacancy clusters. Both groups use supporting arguments concerning length and lattice parameter change, defect cluster observation, or the recovery of hardness and mechanical properties to fortify their position, but neither has been able to prove their case conclusively.

Because additional information is needed to identify uniquely the mobile defect, or defects, in the 150°C stage, a new approach which differs radically from that of previous investigators has been utilized. In addition to the customary postirradiation anneals at pressures equal to or less than 1 bar, irradiated Mo specimens have been subjected to isochronal anneals at high hydrostatic pressures. The reason for this approach is briefly outlined in a qualitative fashion below.

Since any defect, whether it is a vacancy, interstitial, or cluster of either type, increases the specific volume of a crystal, the application of a hydrostatic pressure will raise the energy of a crystal containing such defects more than that of an identical crystal with no defects. This extra strain energy will then provide a driving force for the elimination or annealing of the defect. However, the defect must migrate to be removed, and pressure also affects that process. In the simple case of a migrating vacancy, the atom jumping into the vacancy must pass through a ring of lattice atoms. At its saddle point, this ring of atoms is forced outward and causes a volume increase ΔV . To do this when a pressure P is pushing on the crystal requires an extra amount of energy $P\Delta V$. The term ΔV is commonly referred to

* Paper based on work performed under U. S. Atomic Energy Commission Contract AT(45-1)-1830.

¹ J. Nihoul, in *Symposium on Radiation Damage in Solids and Reaction Materials, Vienna, 1962* (International Atomic Energy Agency, Vienna, 1963), Vol. 1.

² N. F. Pravdyuk and A. M. Ivanov, Atomic Energy Commission Report No. AEC-TR-5263, 1962 (unpublished).

³ S. Veljkovic and N. Milasin, Atomic Energy Commission Report No. AEC-TR-6227/2, 1964 (unpublished).

⁴ M. DeJong and H. B. Afman, *Acta Met.* **15**, 1 (1967).

⁵ J. Moteff and J. P. Smith, in *Flow and Fracture of Metals and Alloys in Nuclear Environments*, Special Technical Publication No. 380 (American Society for Testing Materials, Philadelphia, Pa., 1965), p. 171.

⁶ G. H. Kinchin and M. W. Thompson, *J. Nucl. Energy* **6**, 275 (1958).

⁷ D. E. Peacock and A. A. Johnson, *Phil. Mag.* **8**, 563 (1963).

⁸ M. DeJong and B. L. Wensink, *Phys. Letters* **17**, 200 (1965).

⁹ B. L. Eyre and A. C. Roberts, in *Flow and Fracture of Metals and Alloys in Nuclear Environments*, Special Technical Publication No. 380 (American Society for Testing Materials, Philadelphia, Pa., 1965), p. 188.

¹⁰ M. E. Downey and B. L. Eyre, *Phil. Mag.* **11**, 53 (1965).

¹¹ A. S. Wronski, G. A. Sargent, and A. A. Johnson, in *Flow and Fracture of Metals and Alloys in Nuclear Environments*, Special Technical Publication 380 (American Society for Testing Materials, Philadelphia, Pa., 1965), p. 69.